Computational analysis of residue contributions to coiled-coil topology

Jorge Ramos and Themis Lazaridis*

Department of Chemistry, The City College of CUNY, 160 Convent Avenue, New York, New York 10031

Received 20 March 2011; Revised 4 August 2011; Accepted 9 August 2011
DOI: 10.1002/pro.718
Published online 19 August 2011 proteinscience.org

Abstract: A variety of features are thought to contribute to the oligomeric and topological specificity of coiled coils. In previous work, we examined the determinants of oligomeric state. Here, we examine the energetic basis for the tendency of six coiled-coil peptides to align their α-helices in antiparallel orientation using molecular dynamics simulations with implicit solvation (EEF1.1). We also examine the effect of mutations known to disrupt the topology of these peptides. In agreement with experiment, ARG or LYS at *a* or *d* positions were found to stabilize the antiparallel configuration. The modeling suggests that this is not due to *a*–*a*′ or *d*–*d*′ repulsions but due to interactions with *e*′ and *g*′ residues. TRP at core positions also favors the antiparallel configuration. Residues that disfavor parallel dimers, such as ILE at *d*, are better tolerated in, and thus favor the antiparallel configuration. Salt bridge networks were found to be more stabilizing in the antiparallel configuration for geometric reasons: antiparallel helices point amino acid side chains in opposite directions. However, the structure with the largest number of salt bridges was not always the most stable, due to desolvation and configurational entropy contributions. In tetramers, the extent of stabilization of the antiparallel topology by core residues is influenced by the *e*′ residue on a neighboring helix. Residues at *b* and *c* positions in some cases also contribute to stabilization of antiparallel tetramers. This work provides useful rules toward the goal of designing coiled coils with a well-defined and predictable three-dimensional structure.

Keywords: coiled coils; parallel; antiparallel; crick model; implicit solvation; EEF1.1; molecular dynamics simulations; free energy decomposition; conformational entropy

Introduction

The coiled coil is one of the simplest protein super secondary structure motifs, consisting of two or more α-helices wrapped around each other in a superhelical twist. It occurs in nature as the dominant motif in fibrous proteins and a mediator of oligomerization.[1–3] Most coiled coils are characterized by a heptad repeat commonly denoted by the letters ***abcdefg***, where residues at positions ***a*** and ***d*** are predominantly hydrophobic, while those at the other positions are usually charged or polar. The heptad repeat allows a relatively easy detection of coiled coils in amino acid sequences. Much more difficult to predict are the oligomeric state (dimer, trimer, etc.) and the topology (parallel or antiparallel).[4]

Parallel coiled coils have been studied more extensively, especially in regard to the determinants of oligomeric state specificity. Mutagenesis studies of the GCN4-p1 peptide concluded that packing geometry varies with oligomeric state.[5] Thus, due to restrictions in packing geometry at a given heptad position, different residues will have different oligomeric propensities.[6,7] Recently, we used a molecular dynamics (MD) approach to dissect the oligomerization preferences of four coiled-coil sequences.[8] Our calculations reproduced some generally accepted rules such as the dimer specificity of LEU at ***d***, the tetramer specificity of LEU at ***a***, and the role of nonpolar side chains at positions ***e*** and ***g*** in specifying higher order structures.

Additional Supporting Information may be found in the online version of this article.

Grant sponsor: NSF; Grant number: MCB-0615552; Grant sponsor: NIH (RCMI); Grant number: RR03060

*Correspondence to: Themis Lazaridis, Department of Chemistry, The City College of CUNY, 160 Convent Avenue, New York, NY 10031. E-mail: tlazaridis@ccny.cuny.edu

The determinants of topology are less well understood. Naturally occurring antiparallel coiled-coil dimers contain polar or charged residues at core positions, which are thought to destabilize the parallel topology due to unfavorable electrostatic interactions. For example, the peptide corresponding to residues 468–497 of the C-terminal domain of the *E. Coli* osmosensor ProP contains an ARG at position ***a***[9] and its *Agrobacterium tumefaciens* counterpart has one LYS and one ARG at different ***a*** positions.[10] Crosslinking experiments suggest that an ARG**488-**ILE substitution does not prevent dimerization of the osmosensor but rather may cause reorientation of the coiled-coil helices.[11] In an experimental study of the *Agrobacterium tumefaciens* osmosensor ProP counterpart, the investigators mutated one LYS and one ARG at different ***a*** positions to ILE. The ARG to ILE mutations resulted in loss of topological specificity while replacing both the ARG and the LYS with ILE resulted in a parallel coiled-coil dimer. The ARG[***a***] forms stabilizing interstrand salt bridges with two ASP residues. Mutation of the two ASP to ALA had a modest impact on the function of the protein.[10] Another interaction of this type involves a ***d*** position ARG in the helical arm of *E. coli* seryl tRNA synthetase forming a salt-bridge with a GLU residue at a ***g***' position.[12] In the parallel orientation, these electrostatic interactions would shift from ***d***/***g***′ to ***d***/***e***′. This type of interaction occurs often in natural antiparallel coiled coils and might help specify helix orientation. However, mutagenesis failed to see important energetic contributions of salt bridges involving interior residues to coiled-coil stability and structure.[13]

Electrostatic interactions between solvent-exposed residues also affect topology. In an antiparallel dimer, the residues at positions ***e*** and ***e***′ are on one side and residues at positions ***g*** and ***g***′ are on the other. Thus, a design where the ***e*** and ***g*** positions have opposite polarities would result in interchain electrostatic attraction in the parallel topology, whereas residues with the same polarity would stabilize the antiparallel orientation.[14,15] The importance of electrostatic interactions was also evident in the case of the C-terminal domain from bovine inhibitor protein of F1 ATPase, which forms an antiparallel coiled-coil dimer but switches to tetramer above pH 6.5.[16]

Another factor that affects the alignment of the helices is packing. For example, ILE at ***d*** positions are poorly accommodated at the core of dimeric parallel coiled coils,[5] but a favorable packing environment can be created by matching ILE with ALA at some of the core ***a***/***d*** layers in the antiparallel conformer.[17] A pattern of ILE at ***d*** with ALA at ***a*** creates a cavity in the interior of the parallel homodimer, while it generates a well packed interface in the antiparallel homodimer.[6] The effect of steric matching is more pronounced in the antiparallel dimer formed by a fragment of the C-terminal domain of the HIV-1 regulatory protein Vpr. The most prominent feature is a pair of TRP[***a***]/HIS[***d***] stacking interactions.[18] In a parallel coiled-coil dimer, two TRP side chains would be side-by-side, which is destabilizing due to the small space between the two helices.

Antiparallel coiled-coil trimers are rare. One of the few available structures is an artificial construct made from the GCN4-p1 peptide with a central ASN16***a*** mutated to ALA.[19] The change in orientation was attributed to the cavity present in the parallel trimer. This is supported by the observation that when the cavity was occupied by a benzene molecule, the parallel trimer was stabilized.[20] Schnarr and Kennan[21] have designed antiparallel coiled-coil trimers where the choice of side chain patterning promotes the desired orientation by means of steric matching. Coil-Ser was a synthetic peptide designed to form a parallel coiled-coil dimer, but crystallization showed it to be an antiparallel trimer.[22] This was attributed primarily to hydrophobic interactions and possibly to helix macrodipole interactions, rotamer energies, and steric effects.

Antiparallel coiled-coil tetramers are often characterized by the presence of apolar amino acids at either the ***e*** or ***g*** position in the heptad repeat and form two pairs of pseudo-equivalent faces, two ***g***/***c*** faces and two ***b***/***e*** faces. Betz and DeGrado[23] used those structural features for the design of antiparallel four helix bundles. When compared with the parallel topology, side chain packing is much more efficient in the antiparallel coiled-coil tetramer.[24] The packing efficiency is more likely to make strong contributions when the side chains occupying the ***a*** and ***d*** positions are significantly different in size. Antiparallel coiled-coil tetramers such as the heterogeneous nuclear ribonucleoprotein (hnRNP) contain LEU, ILE, and VAL at the core positions, thus the packing effect will likely make only minor contributions in determining helix orientation.[25] A single substitution at a solvent-exposed site (GLU20***e***CYS) changed the topology of the tetrameric GCN4-LI peptide[5] from parallel to antiparallel.[24]

An important structural feature in antiparallel coiled coils is the heptad register shift between neighboring helices.[26] Recent studies of antiparallel tetrameric coiled coils have identified at least five kinds of interaction patterns directed by hydrophobic repeats of ***a-d*** (1W5K), ***a-d-e*** (2R2V), and ***a-d-g*** (2B22) type.[27] These patterns differ markedly from classical knobs-into-holes packing interactions and the neighboring helices are vertically offset resulting in a variety of interdigitated packing arrangements as opposed to the discrete layers of side chain interactions found in parallel coiled coils. Another recent study of antiparallel coiled-coil dimers highlights the importance of vertical contacts, in addition to the

lateral contacts usually considered.[28] The study focused on the interaction of ***a*** residues on one helix with ***a*** residues above and below it on the other helix (***a***′-***a***-***a***′ triads) and found that certain combinations are lower in energy than others.

Computational techniques could prove useful in recognizing the correct helix orientation of coiled coils. Keating and coworkers[29] used structure- and sequence-based methods to predict the correct topology of coiled coils and achieved up to 81% prediction accuracy. In previous work, we modeled four sequences onto the structures of dimeric, trimeric, tetrameric, and pentameric coiled coils and demonstrated that our free energy calculation protocol using a conformational search can discriminate the correct oligomeric state of homotypic parallel coiled coils.[8] In addition, we used the decomposition of the energy into residue contributions to obtain insights into the oligomeric propensity of different residue types at different heptad positions. In this work, we consider six coiled-coil sequences that form antiparallel coiled-coil dimers, trimers, and tetramers. In order to examine the full length sequence of each structure set and to remove any bias from using experimental structures for the native topology, we build both parallel and antiparallel configurations for these sequences using Crick's model.[30] We evaluate their relative stability using MD simulations with the effective energy function EEF1.1.[31] and individual residue contributions are computed to obtain new insights that might contribute to the design of coiled coils with a well defined and predictable three-dimensional structure.[32]

Table I. *Free Energy Estimates for All Sequences Studied*

Topology		Parallel	Antiparallel
1R48 DIMER	**A**		
Average eff. int.		−150.57 ± 0.29	−155.52 ± 0.31
$-T\Delta S^{conf}$		6.44 ± 0.15	5.95 ± 0.08
Free energy		−144.13 ± 0.33	−149.56 ± 0.32
1X9V DIMER	**B**		
Average eff. int.		−67.45 ± 0.16	−67.94 ± 0.17
$-T\Delta S^{conf}$		4.23 ± 0.08	2.76 ± 0.17
Free energy		−63.22 ± 0.18	−65.18 ± 0.24
1RB4 TRIMER	**C**		
Average eff. int.		−129.08 ± 0.26	−128.39 ± 0.26
$-T\Delta S^{conf}$		9.64 ± 0.02	6.87 ± 0.23
Free energy		−120.01 ± 0.26	−121.51 ± 0.35
1COS TRIMER	**D**		
Average eff. int.		−141.61 ± 0.26	−141.15 ± 0.25
$-T\Delta S^{conf}$		11.01 ± 0.19	6.10 ± 0.26
Free energy		−130.61 ± 0.32	−135.05 ± 0.36
1W5K TETRAMER	**E**		
Average eff. int.		−117.67 ± 0.24	−120.54 ± 0.24
$-T\Delta S^{conf}$		13.59 ± 0.15	11.76 ± 0.14
Free energy		−104.07 ± 0.28	−108.78 ± 0.28
1TXP TETRAMER	**F**		
Average eff. int.		−121.35 ± 0.26	−121.78 ± 0.29
$-T\Delta S^{conf}$		12.45 ± 0.06	9.28 ± 0.10
Free energy		−108.90 ± 0.27	−112.50 ± 0.31

The effective energy is an average during two 0.8 ns (400 frames) Nosé-Hoover MD simulations. The configurational entropy has been evaluated on 15 frames per MD run. All entries are in units of Kcal/mol per helix. Error bars are the standard deviation of the mean value over the trajectory.

Results

The overall free energy differences between parallel and antiparallel constructs are given in Table I. The antiparallel topology is correctly predicted for the six sequences studied, although the free energy difference between the parallel and antiparallel configurations is small. Decomposition of the free energy into residue contributions is given in Tables S1–S6 in Supporting Information. The contribution of each residue to the free energy is calculated as the intraresidue effective energy plus one half of the effective interaction energy of the residue with its surroundings plus the side chain entropy (CONF). The effective energy is further decomposed into van der Waals (VDW), electrostatics (ELEC), solvation (SOLV), and bonded energy (BOND) to correlate with the structural features observed in the average structure or certain frames from the MD simulation when appropriate.

Dimers

Supporting Information Tables S1 and S2 reveal that one of the largest contributions to antiparallel specificity comes from Ile or Val residues at ***d*** positions. ILE6***d*** is by far the largest determinant of the antiparallel alignment of the 1R48 sequence, primarily due to the BOND term. Further decomposition of this term in ILE6***d*** identified the $\chi 1$ bonds as the source of the highest energy, both of which have much lower energies in the antiparallel structure. The antiparallel arrangement is also favored by ILE13***d*** in the 1R48 sequence (due to mostly VDW) and VAL6***d*** in the 1X9V sequence (due to VDW and BOND). This observation is consistent with the empirical rule that beta-branched side chains pack poorly at position ***d*** of parallel coiled-coil dimers, thus favoring the antiparallel arrangement. It seems that placing two beta branched residues side by side in the parallel coiled-coil dimer induces steric repulsion, which may appear as VDW or BOND energy depending on the structural context. This idea has been used to drive heterodimeric specificity in a designed peptide targeting a metastable coiled-coil domain.[33]

According to conventional wisdom, ARG and LYS at ***a*** or ***d*** positions provide antiparallel dimer specificity due to electrostatic repulsion in the parallel dimer. However, in our parallel model of the 1R48 sequence the charged portions of these side chains point toward the solvent, minimizing electrostatic repulsions between them. ARG24***a*** favors the antiparallel conformation by 0.46 kcal/mol, but this

is due to SOLV and CONF terms; ELEC favors the parallel arrangement. In addition, other interactions seem to be playing a role. The solution structure of the 1R48 antiparallel dimer shows ARG24***a*** and a pair of ASP residues (ASP14***e*** and ASP11***b***) in the neighboring helix within range for hydrogen bond formation.[9] The interactions of ARG24***a*** in our minimized average model are summarized in Figure 1(A). In this model, ARG24***a*** adopts a rotameric state that allows it to interact only with ASP14***e***. The stabilizing effect from the ELEC term is not obvious if only ARG24***a*** is examined but all three residues combined (ARG24***a***, ASP14***e***, and ASP11***b***) make a favorable ELEC contribution to the antiparallel arrangement. Other interactions are observed in the parallel 1R48 dimer: the guanidinium group of ARG24***a*** comes within interacting distance from the ε-amino group of LYS23***g***′ [Fig. 1(B)]. The latter favors the antiparallel structure by 0.91 kcal/mol, partly due to electrostatic interactions with ASP12***c*** and GLU16***g*** from the neighboring helix in the antiparallel conformer. Thus, for GLU16***g***, LYS23***g***, and ARG24***a***, the 1R48 sequence provides favorable interactions in the antiparallel conformer and an unfavorable environment in the parallel conformer [Fig. 1(C,D)].

Bulky residues (HIS or TRP) at core positions also favor the antiparallel topology. The results may not be generalizable, because the instances where HIS or TRP are found in the sequences studied occur at the edge of the coiled coil. HIS31***a*** in the 1R48 sequence favors the antiparallel configuration in part due to steric effects. Placing two HIS at the core of a coiled-coil dimer is unfavorable while matching it with a smaller residue will result in a larger number of allowed rotamers (−0.16 kcal/mol CONF) and better packing (−0.73 kcal/mol BOND). The ELEC and SOLV terms also favor the antiparallel topology. We noted that when ILE at ***d*** is matched with HIS at ***a*** in the antiparallel structure, both side chains retain their initial rotamers. However, when HIS was matched with HIS (in the parallel structure) one of the residues flipped.

The 1X9V sequence has a TRP[***a***] near the N-Terminus and a HIS[***d***] near the C-terminus forming a stacking interaction in the antiparallel structure.[18] In our model, SCWRL3.0 built TRP3***a*** in a rotamer that differs from that observed in the PDB structure. However, during the MD simulation TRP3***a*** and HIS20***d*** came very close to a stacking arrangement. The contribution to antiparallel specificity from this residue pair is quite large, 2.38 and 0.68 kcal/mol from TRP3***a*** and HIS20***d***, respectively, the largest contributions coming from the ELEC and BOND terms.

Trimers

Very few structures of antiparallel coiled-coil trimers are available at present. Their asymmetry complicates our analysis because one of each three equivalent residues is in a different structural environment. In this work, the parallel helices are called A and C and the antiparallel one B. The energy calculations were done separately for each helix, but the average value is reported in Supporting Information Tables S3 and S4. We noted that the three helices do not contribute equally to the reported average free energy, and the differences are sometimes large.

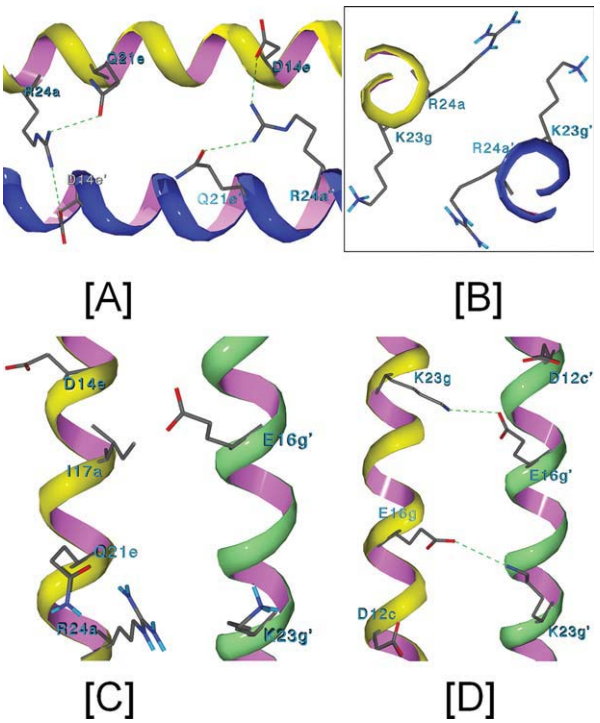

Figure 1. Comparison of electrostatic interactions in parallel and antiparallel structures of 1R48. A: Interactions between ARG24***a*** and the residues ASP14***e***′ and GLN21***e*** in the average structure. Hydrogen bonds (green dotted lines) drawn with Swiss Viewer with a 2.76 Å detection threshold. B: Top view of ARG24***a*** and LYS23***g***′ in the parallel 1R48 model. The two side chains are close enough to interact, which results in an unfavorable ELEC term. C: Parallel 1R48 model showing residues within interacting distance of LYS23***g*** and GLU16***g***. For clarity, only the interactions on one side of the coiled coil are shown. D: Antiparallel 1R48 model showing how LYS23***g*** and GLU16***g*** interact. Note that ASP12***c*** can also participate in electrostatic interactions with LYS23***g*** from the opposite helix. [Color figure can be viewed in the online issue, which is available at wileyonlinelibrary.com.]

The 1RB4 antiparallel trimer resulted from a core ASN to ALA mutation on a parallel dimer. It was reasonably surmised that this flip was due to an energetically unfavorable cavity formed by the Ala residues in the parallel dimer or trimer.[19] In our calculations, the residue in question (ALA17***a***) indeed favors slightly the antiparallel topology in terms of VDW and SOLV. In the antiparallel structure, ALA17***a*** and LEU13***d*** form one ALA/ALA/LEU and one LEU/LEU/ALA layer. However, LEU13***d*** does not favor the antiparallel topology. More detailed analysis

shows that the VDW stabilization of ALA17**a** actually comes from interactions with LEU14***e***. Because of the asymmetry of the structure, LEU14***e*** and ALA17***a*** (from helix A and helix B) form two identical ALA/LEU layers very similar to what we would see in the core of an antiparallel dimer. This points to the importance of ***a***/***e***′ and ***d***/***g***′ interactions in stabilizing antiparallel coiled-coil trimers. Overall, the remaining core ***a*** and ***d*** residues do not favor the antiparallel topology, except for a couple of LEU residues at ***a*** and ***d*** positions in the 1COS sequence.

The 1COS sequence contains a TRP at an ***a*** position near the N terminus. As observed in dimers, TRP3**a** favors the antiparallel conformer by 1.47 kcal/mol due to VDW, ELEC, and BOND terms. This seems to be due mainly to steric reasons, which could be even more unfavorable if the TRP side chains were located in the middle of the sequence. Although not encountered in the six structures studied here, TRP[***d***] might behave similarly. Such features are observed in naturally occurring antiparallel coiled-coil trimers, such as the repetitive segments of spectrin.[34] This structure contains HIS at ***a***, PHE at ***d***, and TRP at ***d***.

Another important factor stabilizing the antiparallel topology is surface salt bridges. In the 1RB4 sequence, there is a LYS28***e***-GLU23***g***′ and a LYS16***g***-Glu21***e***′ salt bridge in the parallel structure and a LYS28***e***-GLU7***e***′ and a LYS9***g***-Glu23***g***′ salt bridge in the antiparallel structure. In our calculations, five of these six residues stabilize the antiparallel conformer (Supporting Information Table S3). This may be due to the orientation of the side chains. The salt-bridged sidechains in the antiparallel conformer are in an extended conformation and point toward each other, while the parallel structure places them pointing in roughly the same direction. Thus, salt bridge formation in the parallel topology requires larger deviations from the default rotamers [compare Fig. 2(A) with Fig. 2(B,C)].

Many surface salt bridges are also observed in the 1COS sequence. In the parallel conformer, LYS9***g***, LYS16***g***, and LYS23***g*** interact with GLU14***e***, GLU21***e***, and GLU28***e***, respectively, in three faces of the coil. In the antiparallel conformer, these interactions occur only on one of the faces (the ***e***/***g*** face). One would thus expect the parallel structure to be more stable. However, our calculations indicate that these three LYS all favor the antiparallel conformer by 0.56, 0.52, and 1.01 kcal/mol, respectively. VDW and ELEC favor the parallel conformer, but SOLV and CONF, which favor the antiparallel conformer, dominate (the corresponding side chain entropy contributions are −1.68, −1.45, and −1.39 kcal/mol). Thus, the structure with the maximal number of salt bridges is not always the most stable.

The antiparallel trimer structure also optimizes ***b***-***b***′ interactions, which have no counterparts in the parallel structure. For example, TYR18***b*** provides a small contribution to the antiparallel alignment (0.22 kcal/mol). Energy calculations on the individual helices indicate that TYR18***b*** from helices A and B contribute to the antiparallel preference while TYR18***b*** from helix C slightly opposes it (because it cannot participate in a ***b***-***b***′ interaction). The hydrogen bond between the TYR18***b*** of helix A and helix B is stable enough to be detected in the average structure [See Fig. 2(D)].

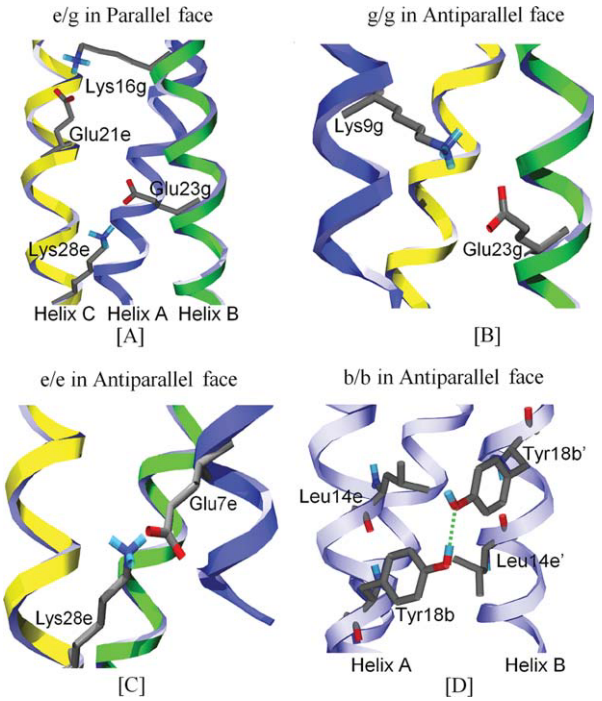

Figure 2. Electrostatic interactions of the trimeric coiled-coil 1RB4. The LYS-GLU salt bridges have different stability depending on the directionality of the interacting side chains. In the parallel topology (A) the alignment of the side chains is not optimal for salt bridge formation. It is so in the antiparallel topology (B and C) where the side chains naturally point in opposite directions. D: Hydrogen bond between TYR18***b*** and TYR18***b***′. The side chains interact favorably by assuming their default rotamers. [Color figure can be viewed in the online issue, which is available at wileyonlinelibrary.com.]

Tetramers

For parallel coiled coils, it is known that LEU[***a***] and ILE[***d***] favor tetramers. The present calculations further show that LEU[***a***] favors antiparallel tetramers in both sequences examined (more clearly so in 1W5K). The extent of this specificity varies and seems to be influenced by the flanking ***e*** and ***d*** residues in the neighboring helix. For example, LEU9***a*** in the 1W5K sequence favors antiparallel by 0.62 kcal/mol. Favorable interactions come from the nearest core residue (ILE26***d***) with comparable contributions from the hydrophobic portion of LYS27***e***. We noted an enhancement of this effect when the ***e***

residues are more hydrophobic. For example, LEU23***a*** favors antiparallel by 0.83 kcal/mol, with favorable interactions coming from ILE12***d*** and LEU13***e*** [Fig. 3(A,B)]. VAL16***a*** in the 1TXP tetramer behaves similarly, in that it exhibits favorable VDW contacts with LYS13***e*** in the opposite helix.

ILE[***d***] sometimes favors the antiparallel conformer and sometimes is indifferent depending on the structural context. For example, ILE5***d*** in 1TXP favors the antiparallel conformer by 1.12 kcal/mol. In the antiparallel structure, ILE5***d*** interacts with LEU23***a*** and ASN22***g*** from neighboring antiparallel helices, whereas in the parallel structure it can interact with a LYS6***e*** from a neighboring helix. Our results indicate that ASN at ***g*** in the antiparallel structure has a more favorable VDW term than LYS at ***e***. It may be that the directionality of the interacting side chains is more relevant than their identity.

In the 1W5K sequence, it is the GLU20***e*** to CYS substitution, which triggers the antiparallel topology. CYS20***e*** favors the antiparallel topology, mostly due to SOLV and CONF. We also built a model for the wild-type sequence and found that a GLU at that position favors the parallel conformer due to ELEC. TYR17***b*** residues pack against the surface of the coiled coil in 1W5K [Fig. 3(C)], whereas in the wild type, the TYR rings point towards the solvent [Fig. 3(D)]. The two CYS20***e*** fit better than two GLU20***e*** within the available space, allowing TYR17***b*** to shield residue 20***e*** from the solvent. The ELEC term of GLU20***e*** in the wild type is unfavorable for the antiparallel conformer, because it places the two GLU20***e*** carboxyl groups close to each other.

In some cases, electrostatic interactions involving ***b*** and ***e*** residues seem to play a role in the antiparallel tetramers. For example, ASP17***b*** in the 1TXP sequence favors antiparallel by 0.66 kcal/mol, mostly from ELEC. The most significant component is from interactions with LYS13***e*** from the neighboring helix. Electrostatic interactions of the ***b-e′*** type are also observed in the structure of another antiparallel tetrameric coiled-coil.[35]

Discussion and Conclusions

In previous work, we demonstrated that our free energy calculation protocol can discriminate the correct oligomeric state of homotypic parallel coiled coils.[8] Analysis of individual residue contributions resulted in an extended set of empirical rules for the oligomeric propensity of many residues at different heptad positions. Here, we applied the same protocol to six coiled-coil sequences that form antiparallel dimers, trimers, and tetramers. Again, the correct orientation was predicted for the sequences considered here, although the differences in free energy were small. A more complete treatment would include consideration of different oligomeric states and different topologies at the same time, but this was beyond the scope of this work.

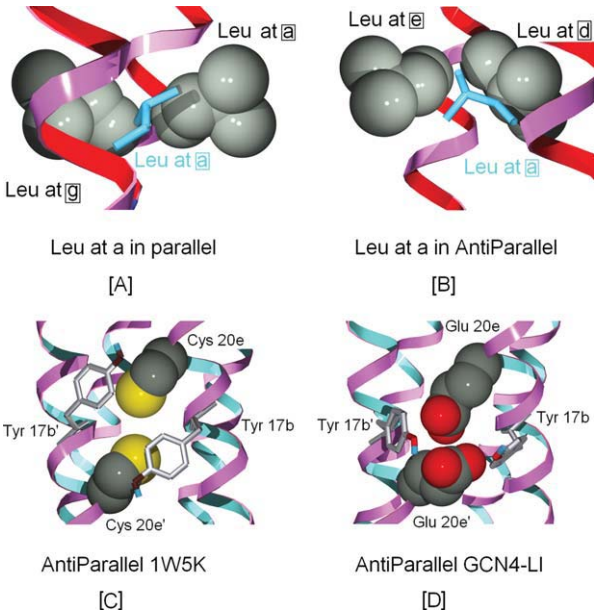

Figure 3. Structural determinants of the 1W5K antiparallel tetramer. A: LEU at ***a*** packing in antiparallel and [**B**] parallel tetramer. The flanking residue at position ***e*** in antiparallel, ***g*** in parallel might be more significant in the antiparallel conformer in terms of VDW. C: Side view of the packing of TYR17b and CYS20e in the 1W5K tetramer. There are two such clusters in an antiparallel coiled-coil tetramer. For clarity, only the front cluster is shown. D: For comparison: packing of TYR17***b*** and GLU20***e*** in an antiparallel GCN4-LI model. Notice that GLU20***e*** is too bulky for its available packing space. [Color figure can be viewed in the online issue, which is available at wileyonlinelibrary.com.]

To ensure that there is no bias in our results, we repeated the calculations for a sequence that in its native form is a parallel coiled coil: the well-known GCN4p1 dimer (PDB code 2ZTA). Both parallel and antiparallel models were built using Crick's equations. The antiparallel dimer was built so that MET3***a*** and LEU27***d*** have the same z coordinate. As can be seen in Table S7 in Supporting Information, the parallel topology is clearly favored. The largest contributions come from the LEU[***d***] residues, in agreement with the results obtained above.

Our theoretical approach clearly involves many approximations. However, the fact that it can discriminate the correct oligomeric state[8] and topology (Table I), as well as the fact that it can reproduce many empirically established rules on the oligomeric and topological propensity of certain amino acid residues at certain positions, support its credibility. Naturally, experimental tests of the theoretical predictions would be valuable.

Our investigation on the determinants of helix orientation yields conclusions that are in agreement with previously reported observations. Because the antiparallel coiled coils incorporate mixed layers, this adds more complexity to their design as the same residue will behave differently depending on

the nature of the interacting partner. Thus, we have expanded the analysis to include interacting amino acid pairs in addition to single residues. The main conclusions are as follows.

1. ARG[***a***] and LYS[***a***] provide antiparallel dimer specificity in the sequences examined here. Placement of these residues at position ***d*** has nearly the same effect. Our calculations suggest that ARG and LYS at ***a*** or ***d*** may not be on their own sufficient to destabilize the parallel dimer structure, as the charged portions of these side chains point toward the solvent. To attain specificity for a single orientation it might be necessary to place residues at ***e***′ or ***g***′ that form unfavorable interactions with the ***a*** or ***d*** position residues in the undesired orientation. That is, ARG and LYS at ***a*** would require ARG or LYS at the ***e***′ position, while ARG and LYS at ***d*** would require ARG or LYS at the ***g***′ position to destabilize the competing parallel structure. For example, in the parallel 1R48 dimer, the guanidinium group of ARG24***a*** comes within interacting distance of the ε-amino group of LYS23***g***′. Such an interaction yields an unfavorable ELEC term for the parallel model, effectively shifting the equilibrium toward the antiparallel orientation.
2. ILE[***d***] is known to disfavor parallel dimers. The present results show that it is better tolerated in the antiparallel orientation. However, this preference can be reversed if paired with a β-branched side chain in the complementary ***a*** position. VAL[***d***] likely behaves in the same way as ILE[***d***]. There is one instance (VAL6***d*** in 1X9V) where VAL[***d***] prefers the antiparallel orientation.
3. LEU[***d***] and ILE[***a***] strongly confer dimer specificity. In regard to topology, all LEU[***d***] in the dimers were found to favor the parallel conformer. This was also true for two of the three ILE[***a***]. Thus, a sequence that places ILE[***a***] and LEU[***d***] in contact with each other should be avoided when attempting to design an antiparallel homodimer.
4. TRP[***a***] favors antiparallel dimers or trimers.
5. We have found two HIS at core positions favoring the antiparallel topology but both occur at the edge of the coiled coil and this result may not be generalizable.
6. As observed in dimers, TRP[***a***] favors antiparallel topology. Although not encountered in the six structures studied here, TRP[***d***] might behave similarly. Features such as this can be found in naturally occurring antiparallel coiled-coil trimers such as the repetitive segments of spectrin.[34] This structure contains HIS at ***a***, PHE at ***d***, and TRP at ***d***. Thus the strategic placement of such residues at core positions is one of the most straightforward methods for the design of antiparallel coiled-coil trimers.
7. Electrostatic interactions involving ***e*** and ***g*** residues are stronger in the antiparallel trimers than in their parallel counterparts. The reason is that the side chain pairs are better aligned for interaction in the antiparallel topology. Similar interactions in the parallel topology require larger deviations from the default rotamers. In the 1COS sequence, the protonated GLU at ***e*** are a main determinant of antiparallel topology, because they can interact favorably while retaining low energy rotamers. Here, it was observed that the structure with the maximal number of salt bridges is not always the most stable. Stability depends on a delicate balance of electrostatic, solvation, and conformational entropy terms.
8. LEU[***a***] favors antiparallel tetramers but the extent of this specificity is heavily influenced by the flanking ***e*** residue in the neighboring helix. We found the pair LEU[***a***]-LYS[***e***′] to be particularly stabilizing. ARG at an ***e***′ position might have the same effect.
9. VAL[***a***] behaves a lot like LEU[***a***] due to similarities in their —C—$(CH_2)_2$ unit. We noted one instance where VAL16***a*** in the 1TXP tetramer provides favorable VDW contacts for LYS13***e*** in the opposite helix.
10. ILE[***d***] favors antiparallel tetramers when combined with certain flanking ***g*** residues in the neighboring helix. We found ILE[***d***] combined with ASN at ***g***′ to fit this requirement.
11. In some cases, electrostatic interactions involving ***b*** and ***c*** residues make some contribution in antiparallel tetramers.

Our investigation of the individual residue contributions to the free energy provides new insights that could help in the design of coiled coils with a well-defined and predictable three-dimensional structure. Some trends are consistent with previous results established experimentally. For example, core residues known to stabilize a certain parallel oligomeric state will disfavor the antiparallel conformer. We also noted that polar and charged side chains have greater impact in controlling the topology of antiparallel coiled coils compared with their parallel counterparts.

The ultimate goal in this field is prediction of oligomeric state and topology of coiled coils from sequence alone. Given the complexity and context dependence we observed in this work, this goal seems nontrivial. One avenue for future work could be the application of the present methodology to many more sequences for the extraction of simplified potentials that could be used for scoring all possible states of a given sequence. Of course, experimental mutagenesis studies will continue to be invaluable.

Methods

Model systems

Six antiparallel coiled coils were chosen as model systems in this work, two dimers, two trimers, and two tetramers. The selection was arbitrary. PDB code 1R48[9] is a dimer corresponding to residues 468–497 of the C-terminal domain of the osmosensor ProP. Our model contains 30 residues, from GLY2***g*** to HIS31***a***, in addition to the acetyl (ACE) and *N*-methylamide (CBX) caps. PDB code 1X9V[18] is a dimer, residues 52–96 of the C-terminal domain of the HIV-1 regulatory protein Vpr. The average of the 10 NMR structures indicates that only a short segment of the peptide is folded and the rest is in a random coil conformation. Our model contains 20 residues. PDB code 1RB4[19] is an ASN16ALA mutant of the GCN4 coiled-coil parallel dimer, which forms an antiparallel trimer. The structure reveals that steric matching of large and small (LEU and ALA) side chains might play a role in directing the antiparallel topology. With the addition of the acetyl cap, our coiled-coil model shifts the numbering scheme by +1 compared with the PDB version. PDB code 1COS[22] contains four heptads similar to (LaEbAcLdEeGfKg)$_n$. It was originally designed to mimic the structural features of the tropomyosin coiled-coil dimer. A few modifications to the sequence resulted in an antiparallel coiled-coil trimer. Our model includes the full sequence. PDB code 1W5K[24] corresponds to a mutant of the GCN4-LI sequence (a parallel tetrameric coiled coil). The substitution of a single solvent-exposed glutamic acid residue (GLU20***e*** to CYS) resulted in an antiparallel tetramer. PDB code 1TXP[25] corresponds to the oligomerization domain of the hnRNP antiparallel tetramer. Our model coiled coil contains the full length of the 1TXP peptide plus acetyl and *N*-methylamide caps, which shifts the numbering scheme by one compared with the PDB version. An average of the 20 NMR structures retrieved from the PDB indicates that all but the last four residues in the sequence are helical. These last residues are beyond the oligomerization interface and we built them in a helical conformation.

Generation of coiled-coil structures

Although backbone coordinates can be obtained from the PDB and different sequences can be threaded onto them, this approach places limitations on the length of the coiled coils that can be studied by computational techniques. If experimental structures are to be used, all representative structures must be available in a sequence length that can accommodate the sequence being studied. The Protein Data Bank does not have enough structures to put together every possible coiled-coil set without having to truncate most sequences. For example, it is not yet possible to obtain a complete set of dimeric, trimeric, and tetrameric coiled coils that can accommodate the full 46 residue sequence of the Cartilage Oligomeric Matrix Protein (1VDF). The results from such methods could also be biased depending on the differing resolution of the crystal structures; the structure with the highest resolution will probably appear to have higher stability.

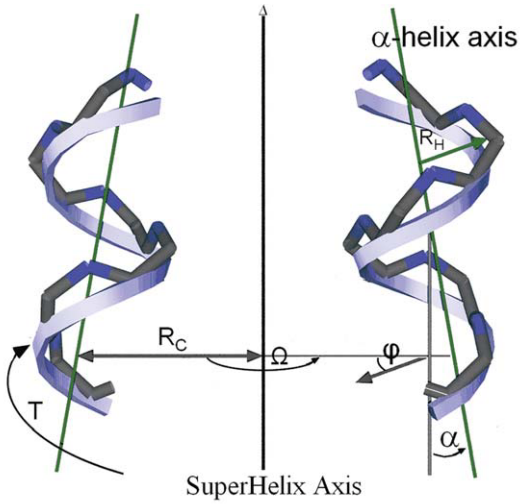

Initial Helix Parameters Atom Type	R_H, Å		dZ, Å
N	1.61		-0.05
Cα	2.27		+1.23
C	1.68		+0.36
Coiled Coil Parameters			
Oligomeric State	R_C, Å	P_C, Å	Ω
Dimer	4.9	148	180^0
Trimer	6.7	175	120^0
Tetramer	7.6	205	90^0

Figure 4. Structural parameters of an ideal coiled coil. The coiled-coil frame rotates in the direction of the parameter $T = 2\pi\ dZ/P_C$. The coiled-coil pitch, P_C, is related to the tilt angle, α, of the component helices by $\alpha = 2\pi\ R_C/P_C$. [Color figure can be viewed in the online issue, which is available at wileyonlinelibrary.com.]

In this work, backbone coordinates were built using Crick's mathematical model for an ideal coiled coil.[30] The parameters of the model are summarized in Figure 4. For simplicity, we will illustrate our general approach using a parallel dimeric coiled coil as an example. A straight helix with 3.5 residues per turn is generated along the *Z* axis. The 3.5 residue/turn periodicity positions each ***a*** and ***d*** residue such that they line up along the helical axis rather than spiraling around the helix as in a canonical α-helix. The atomic coordinates X_i, Y_i, and Z_i, for the backbone atoms in the straight helix are given by,

$$\begin{aligned} X_i &= R_H \sin(\theta t + \varphi) \\ Y_i &= R_H \cos(\theta t + \varphi) \\ Z_i &= Z_{i-1} + dZ \end{aligned} \qquad (1)$$

where the value of θ is 4π/21 radians, the parameter t runs over integral values generating three backbone atoms per residue (21 atoms for every two helical turns), and the values of R_H and dZ depend on the atom type (N, Cα, C). The parameter φ is chosen to position the ***a*** and ***d*** residues toward the center of the coiled coil and is determined by the heptad assignment of the first residue in the sequence.

The helix generated by Eq. (1) is then translated along the X axis by a value equal to the coiled-coil radius and given a left-handed twist using Crick's equations for an ideal coiled coil. The second helix is generated by translating the initial helix along the X axis by a value equal to the coiled-coil radius, rotating it by 180° about the coiled-coil axis and giving it a left-handed twist creating the dimeric coiled coil.

These operations do not change the periodicity of the helix generated by Eq. (1). Thus, if the initial helix had a periodicity of 3.6 residues/turn as in a canonical α-helix the ***a*** and ***d*** residues would drift away from the core region and rarely interlock. The atomic coordinates X_C, Y_C, and Z_C, of the coiled-coil backbone atoms are given by,

$$\begin{aligned} X_C &= [R_C\cos(T+\Omega)] + [X_i\cos(T+\Omega)] \\ &\quad + [Y_i\cos\,\alpha\,\sin(T+\Omega)] \\ Y_C &= [-R_C\sin(T+\Omega)] - [X_i\sin(T+\Omega)] \\ &\quad + [Y_i\cos\,\alpha\,\cos(T+\Omega)] \\ Z_C &= Z_i + Y_i\sin\,\alpha \end{aligned} \qquad (2)$$

where the angular and spatial separations of the component helices in the coiled coil are denoted by Ω and R_C, respectively. The parameter α is the tilt angle of the component helices and is obtained by $\alpha = 2\pi\ R_C/P_C$, where P_C is the coiled-coil pitch. The angular displacement of the initial helix in the coiled-coil frame is given by $T = 2\pi\ (Z_H - Z_0)/P_C$.

The angular separation Ω for a dimeric coil takes the values of 0° and 180° for helix A and B, respectively. For trimeric coils, Ω has values of 0°, 120°, and 240°, while in tetrameric coils Ω has values of 0°, 90°, 180°, and 270°.

The starting values for the coiled-coil parameters are taken from structures with PDB code 2ZTA for dimer, 1CE0 for trimer, and 1GCL for tetramer. The angular separation is nearly invariant for coiled coils of the same oligomeric state although small variations have been observed for some antiparallel coiled coils. The spatial separation and tilt angle also vary slightly. The effective energy was found to be more sensitive to the spatial separation than the tilt angle but the initial parameters were found to be close enough to yield an effective energy minimum. Increasing or decreasing the coiled-coil radius resulted in the test structures moving away from the effective energy minimum. Small adjustments are expected to occur as the structures relax during the MD simulations to account for the differences between the ideal and experimental parameters.

The antiparallel coiled coils were built in the same manner as their parallel counterparts but the initial helix parameters were reversed and the Z displacement offset by a multiple of 1.54 Å for helices that run in the opposite sense to ensure interlocking of ***a*** and ***d*** residues (1.54 Å is the change in the helical Z coordinate per residue added). For example, helix B in the antiparallel dimer is axially displaced relative to helix A so that each turn of helix B runs roughly midway between two adjacent turns in helix A. When the structure is known, the Z displacement offset can be obtained by multiplying the number of unmatched residues at the termini by 1.54 Å. The effective energy is very sensitive to the value of the Z displacement offset and that fact can be used to search for the correct value when the structure is not available. A structure is built starting with the two adjacent helices having zero Z displacement and then adding 1.54 Å in subsequent trials. If the Z displacement is too large or too small compared with the correct value the core residues clash. The structure that gives the lowest effective energy corresponds to the one where the core residues fall into place.

The agreement in the backbone between the minimized average models and the X-ray or minimized average NMR structures is quite good with the RMSD of the backbone atoms being: 1R48: 2.44, 1X9V: 1.24, 1COS: 1.06, 1RB4: 1.01, 1W5K: 1.23, and 1TXP: 1.55 Å. The 1R48 dimer has a relatively large RMSD because the minimized average NMR structure is bent toward the ***b***/***e*** surface [9] while our model was built with ideal coiled-coil parameters. Typically, the RMSD converged to the final value within 0.5 ns.

Side chains were built with SCRWL3.0 and its backbone-dependent rotamer library[36] using the atomic coordinates of the neighboring helices as steric boundaries. This procedure does not always reproduce the experimentally observed rotamer, especially for solvent exposed sidechains. In the core, LEU was better reproduced than the β-branched residues ILE and VAL. Certainly, regular MD is not expected to produce an optimal arrangement of side chains. The free energies of the experimental structures tended to be lower than those of the models, especially for X-ray structures, which mean that the discrimination of the native topology would have been much more pronounced if experimental structures were used for it.

Figures were generated using the minimized average structures. The average of the atomic coordinates from each simulation was taken and the resulting structure was subjected to 300 steps of ABNR minimization.

Molecular dynamics simulations

Dimer and tetramer structures were subjected to 1 ns (500,000 steps) Nose-Hoover MD simulations. In the antiparallel trimer structures, one helix is structurally different from the other two and the free energy values for this helix can be significantly different. Thus, the energy calculations for each helix were done separately for each helix. In our model, helices A and C are parallel to each other and helix B is antiparallel to A and C. The trimer simulations were extended to 1.8 ns (900,000 steps) to improve the convergence of the average effective energies. Longer simulations were found to give essentially identical results. Harmonic constraints with a force constant of 2.0 kcal/Å^2 were applied to the backbone α-carbons to keep the structures close to the desired fold. Smaller values of the force constant were found to distort the structure excessively. The nonbonded interactions were updated every 20 dynamics steps, and the coordinate frames were saved every 1000 steps. The structures were allowed to equilibrate during the first 100,000 steps and the rest of the simulation was used for free energy calculations.

Free energy calculations

The relative stability of a structure is related to the free energy change,

$$\Delta G = \Delta W - T\Delta S. \tag{3}$$

where ΔW is the effective energy change and $T\Delta SP$ is the configurational entropy change. The effective energy term is evaluated by the energy function EEF1.1,

$$W = H_{intra} + \Delta G^{solv} \tag{4}$$

where H_{intra}, and ΔG^{solv} are the intramolecular energy and the solvation free energy, respectively.[31] The ΔG^{solv} term is approximated as a sum of contributions from all the atoms in the macromolecule,

$$\Delta G^{solv} = \sum_i \Delta G_i^{solv} = \sum_i \Delta G_1^{ref} - \sum_i \sum_{j \neq 1} \mathbf{f}_i(\mathbf{r}_{ij})\mathbf{V}_j \tag{5}$$

where ΔG_i^{solv} is the solvation free energy of group **i**. Here ΔG_i^{ref} is the solvation free energy in a fully solvent-exposed model compound, and the summation $\Sigma_{j \neq 1} \boldsymbol{f}_i(\mathbf{r}_{ij})\boldsymbol{V}_j$ accounts for the exclusion of solvent around group **i** due the shielding by groups **j**. EEF1.1 is an updated parameterization[37] based on potentials of mean force calculated in explicit solvent.[38] We compute the effective energy W as the average of all frames recorded after the first 100,000 steps of a MD run. Thus, the effective energy of the dimers and tetramers is the average of 400 frames while the effective energy of the trimers is the average of 800 frames.

The configurational entropy would normally be approximated as a sum of translational, rotational, and conformational contributions. However, we are comparing structures with the same number of helices and different topology. Under these conditions, the rotation and translation entropy can be assumed to be invariant. Then the configurational entropy change ΔS can be approximated by the change in side chain conformational entropy contribution ΔS^{conf} alone (CONF).

We compute the S^{conf} term from the probability distribution of each side chain torsional angle, obtained by rotating each of them independently of the others. Except for proline, alanine, and glycine, all side chain χ angles were rotated one at a time at 10° intervals. From the effective energy profiles, we computed the probability of each conformation,

$$p(\omega) = \frac{\exp[-W(\omega)/RT]}{\int \exp[-W(\omega)/RT]d\omega}. \tag{6}$$

where ω denotes one of the sampled side chain conformations and W(ω) is the associated energy. The conformational entropy of a structure is,

$$S^{conf} = -R\sum\nolimits_{N(\chi)} \cdot \left[\int p(\omega)\ln\, p(\omega)d\omega\right] \tag{7}$$

where the summation is over the total number $N(\chi)$ of torsional angles in the protein. The calculation was done on 15 structures obtained from the MD run and the results were averaged. The conformational entropy loss ΔSP^{confP} is the difference between the S^{conf} term of the multimer and the monomer.

The above method of calculating the side chain entropy and the values obtained are similar to those found in the literature,[39–42] except that the probabilities are more often obtained from Monte Carlo sampling rather than systematic search. The approximation of independence of each side chain employed in Eq. (7) has been tested and found to be surprisingly accurate.[40]

References

1. Burkhard P, Stetefeld J, Sergei SV (2001) Coiled coils: a highly versatile protein folding motif. Trends Cell Biol 11:82–88.
2. Lupas AN, Gruber M (1995) The structure of α-helical coiled coils. Adv Prot Chem 70:37–78.
3. Moutevelis E, Woolfson DN (2009) A periodic table of coiled-coil protein structures. J Mol Biol 385:726–732.
4. Grigorian G, Keating AE (2008) Structural specificity in coiled coil interactions. Curr Opin Struct Biol 18: 477–483.
5. Harbury PB, Zhang T, Kim PS, Alber T (1993) A switch between two-, three-, and four-stranded coiled coils in GCN4 leucine zipper mutants. Science 262:1401-1406.

6. Wagschal K, Tripet B, Lavigne P, Mant C, Hodges RS (1999) The role of position a in determining the stability and oligomerization state of α-helical coiled coils: 20 amino acid stability coefficients in the hydrophobic core of proteins. Protein Sci 8:2312–2329.
7. Tripet B, Wagschal K, Lavigne P, Mant CT, Hodges RS (2000) Effects of side-chain characteristics on stability and oligomerization state of a de novo-designed model coiled-coil: 20 amino acid substitutions in position d. J Mol Biol 300:377–402.
8. Ramos J, Lazaridis T (2006) Energetic determinants of oligomeric state specificity in coiled coils. J Am Chem Soc 128:15499–15510.
9. Zoetewey DL, Tripet BP, Kutateladze TG, Overduin MJ, Wood JM, Hodges RS (2003) Solution structure of the C-terminal antiparallel coiled-coil domain from *Escherichia coli* osmosensor ProP. J Mol Biol 334:1063–1076.
10. Tsatskis Y, Kwok SC, Becker E, Gill C, Smith MN, Keates RAB, Hodges RS, Wood JM (2008) Core residue replacements cause coiled-coil orientation switching in vitro and in vivo: structure-function correlations for osmosensory transporter ProP. Biochemistry 47:60–72.
11. Hillar A, Culham DE, Vernikovska YI, Wood JM, Boggs JM (2005) Formation of an antiparallel, intermolecular coiled coil is associated with in vivo dimerization of osmosensor and osmoprotectant transporter ProP in *Escherichia coli*. Biochemistry 44:10170–10180.
12. Cusack S, Berthet-Colominas C, Härtlein M, Nassar N, Leberman R (1990) A second class of synthetase structure revealed by X-ray analysis of *Escherichia coli* seryl-tRNA synthetase at 2.5 Å. Nature 347:249–255.
13. McClain DL, Gurnon DG, Oakley MG (2002) Importance of potential interhelical salt-bridges involving interior residues for coiled-coil stability and quaternary structure. J Mol Biol 324:257–270.
14. McClain DL, Binfet JP, Oakley MG (2001) Evaluation of the energetic contribution of interhelical coulombic interactions for coiled coil helix orientation specificity. J Mol Biol 313:371–383.
15. Monera OD, Kay CM, Hodges RS (1994) Electrostatic interactions control the parallel and antiparallel orientation of α-helical chains in two-stranded α-helical coiled-coils. Biochemistry 33:3862–3871
16. Gordon-Smith DJ, Carbajo RJ, Yang JC, Videler H, Runswick MJ, Walker JE, Neuhaus D (2001) Solution structure of a C-terminal coiled-coil domain from bovine IF(1): the inhibitor protein of F(1) ATPase. J Mol Biol 308:325–339.
17. Gurnon DG, Whitaker JA, Oakley MG (2003) Design and characterization of a homodimeric antiparallel coiled coil. J Am Chem Soc 125:7518–7519.
18. Bourbigot S, Beltz H, Denis J, Morellet N, Roques BP, Mély Y, Bouaziz S (2005) The C-terminal domain of the HIV-1 regulatory protein Vpr adopts an antiparallel dimeric structure in solution via its leucine-zipper-like domain. Biochem J 387:333–341.
19. Holton J, Alber T (2004) Automated protein crystal structure determination using ELVES. Proc Natl Acad Sci USA 101:1537–1542.
20. Gonzalez L,Jr, Plecs JJ, Alber T (1996) An engineered allosteric switch in leucine-zipper oligomerization. Nat Struct Biol 3:510-515.
21. Schnarr NA;Kennan AJ (2004) Strand orientation by steric matching: a designed antiparallel coiled-coil trimer. J Am Chem Soc 126:14447–14451.
22. Lovejoy B, Choe S, Cascio D, McRorie DK, DeGrado WF, Eisenberg D (1993) Crystal structure of a synthetic triple-stranded alpha-helica1 bundle. Science 259:1288–1293.
23. Betz SF, DeGrado WF (1996) Controlling topology and native-like behavior of de novo-designed peptides: design and characterization of antiparallel four-stranded coiled coils. Biochemistry 35:6955–6962.
24. Yadav MK, Leman LJ, Price DJ, Brooks CL,III, Stout CD, Ghadiri MR (2006) Coiled coils at the edge of configurational heterogeneity. Structural analyses of parallel and antiparallel homotetrameric coiled coils reveal configurational sensitivity to a single solvent-exposed amino acid substitution. Biochemistry 45: 4463–4473.
25. Whitson SR, LeStourgeon WM, Krezel AM (2005) Solution structure of the symmetric coiled coil tetramer formed by the oligomerization domain of hnRNP C: Implications for biological function. J Mol Biol 350: 319-337.
26. Gernert KM, Surles MC, Labean TH, Richardson JS, Richardson DC (1995) The Alacoil: a very tight, antiparallel coiled-coil of helices. Protein Sci 11:2252–2260.
27. Liu J, Zheng Q, Deng Y, Li Q, Neville RK, Lu M (2007) Conformational specificity of the *Lac* repressor coiled-coil tetramerization domain. Biochemistry 46: 14951–14959.
28. Hadley EB, Testa OD, Woolfson DN, Gellman SH (2008) Preferred side-chain constellations at antiparallel coiled-coil interfaces. Proc Natl Acad Sci USA 105: 530–535.
29. Apgar JR, Gutwin KN, Keating AE (2008) Predicting helix orientation for coiled-coil dimers. Proteins 72: 1048–1065.
30. Crick FHC (1953) The Fourier transform of a coiled-coil. Acta Crystallogr 6:685–689.
31. Lazaridis T, Karplus M (1999) Effective energy function for proteins in solution. Proteins 35:133–152.
32. Woolfson DN (1995) The design of coiled- coil structures and assemblies. Adv Protein Chem 70:79–112.
33. Barth P, Schoeffler A, Alber T (2008) Targeting metastable coiled-coil domains by computational design. J Am Chem Soc 130:12038–12044.
34. Yan Y, Winograd E, Viel A, Cronin T, Branton CD (1993) Crystal structure of the repetitive segments of spectrin. Sci New Series 262:2027–20XX.
35. Fujiwara Y, Minor DL,Jr (2008) X-ray crystal structure of a TRPM assembly domain reveals an antiparallel four-stranded coiled-coil. J Mol Biol 383:854–870.
36. Canutescu AA, Shelenkov AA, Dunbrack RL,Jr (2003) A graph-theory algorithm for rapid protein side-chain prediction. Protein Sci 12:2001-2014.
37. Lazaridis T (2003) Effective energy function for proteins in lipid membranes. Proteins 52:176–192.
38. Masunov A, Lazaridis T (2003) Potentials of mean force between ionizable amino acid side chains in water. J Am Chem Soc 125:1722-1730.
39. Doig AJ, Sternberg MJE (1995) Side-chain conformational entropy in protein folding. Protein Sci 4: 2247–2251.
40. Hu X, Kuhlman B (2006) Protein design simulations suggest that side-chain conformational entropy is not a strong determinant of amino acid environmental preferences. Proteins 62:739–748.
41. Chellgren BW, Creamer TP (2006) Side-chain entropy effects on protein secondary structure formation. Proteins 62:411–420.
42. Zhang J, Liu JS (2006) On side-chain conformational entropy of proteins. PLOS Comput Biol 2:1586–1591.